International Journal of Heat and Technology
Vol. 41, No. 2, April, 2023, pp. 279-292
Journal homepage: http://iieta.org/journals/ijht

Empirical Relationship Describing Total Convective and Radiative Heat Loss in Buildings

Michał Ryms[1*], Grzegorz J. Kwiatkowski[2], Witold s.M. Lewandowski[1]

[1] Gdansk University of Technology, Faculty of Chemistry, Department of Energy Conversion and Storage, G. Narutowicza 11/12, Gdańsk PL-80-233, Poland
[2] Science Institute of the University of Iceland, Dunhagi 3, Reykjavik 107, Iceland

Corresponding Author Email: michal.ryms@pg.edu.pl

https://doi.org/10.18280/ijht.410201

Received: 6 February 2023
Accepted: 2 April 2023

Keywords:
convective-radiative heat transfer, infrared camera, experiments, empirical equation, vertical plate

ABSTRACT

On the basis of theoretical considerations of convective-radiative heat transfer, a relationship was developed enabling the total convective and radiative heat flux Q_{C+R} emitted from any object at t_w and its surroundings at t_∞ to be calculated from known values of the surface temperature of such an object, i.e., the known temperature difference $\Delta t=t_w - t_\infty$ and average air temperature T_{av}. This relationship is applied to thermal imaging cameras with the aim of developing appropriate software to enhance their measurement capabilities. They can then be used not only for monitoring and measuring temperature, local overheating, heat losses through insulation materials, thermal bridges, constructional defects, moisture, etc., but also for measuring the heat losses from any object, such walls and buildings. This empirical relationship includes constants relating to the object itself, such as its characteristic dimension l, surface area A, emissivity ε and temperature parameters, which depend on t_w, t_∞, Δt and T_{av} and on the physical properties of air. Experimental validation of the proposed relationship, performed for two values of the surface emissivity ε, showing the discrepancies ΔQ_{C+R}=1.75% (for ε=0.884) and 4.85% (for ε=0.932), has confirmed its correctness and its practicability.

1. INTRODUCTION

Heat transfer in air is a complex mechanism involving both convection and radiation. Despite this mutual coexistence, these two means of heat transfer are usually considered separately, and the results obtained for either of them, though most often for convection, described by Newton's equation, are corrected by subtracting the radiant heat flux calculated with the Stefan-Boltzmann equation. On the other hand, when determining heat losses, the calculated radiative heat loss flux is added to the measured convective heat flux. To determine the convective heat flux, it is necessary to know the heat transfer coefficient α, the dimensions l and b of the object under consideration and its surface temperature t_w, as well as the ambient air temperature in the undisturbed area t_∞. In addition, for the radiant flux the temperature of the surrounding walls $t_{ot} \approx t_\infty$ and the surface emissivity ε are also required: this latter quantity should be measured, assumed, or be taken from a set of tables that assign their values to typical surfaces (polished copper, brick, plaster, wood, etc.) [1, 2].

At lower temperatures, convection becomes more important and is of great interest to researchers, even though it involves a much higher level of complexity. This emerges from its physical description, which in the case of free convection requires three conjugate partial differential equations (continuity, Navier-Stokes and Fourier-Kirchhoff), the mathematical methods of solving them, and carrying out the relevant experimentation. These difficulties, far from discouraging researchers, have inspired them to study convection even more intensively. At the same time, the only reward they could count on was scientific satisfaction, because industry was not interested in this low-intensity mode of heat transfer. Times and attitudes have changed, however: the primary aim nowadays is to conserve energy, for example, by limiting heat losses, mainly caused by free convection, especially in the construction, energy and metallurgy industries.

At higher temperatures, radiative heat transfer is more important, for the description of which the Planck, Wien, Stefan-Boltzmann and other equations are necessary [3, 4]. In external heat transfer and for simple spatial configurations, especially at low temperatures, radiation can be described only by the Stefan-Boltzmann equation, but its practical use is troublesome. To determine the radiative heat flux from this equation, it is not enough to know the temperatures of the heating surface t_w and the surroundings t_∞, and the emissivity ε. One also needs to know the temperature of surrounding objects, as well as the humidity and pressure of the air. In the case of internal heat transfer, however, e.g. in heat exchangers, engine cylinder channels or combustion chambers, when the areas of a heated surface A_w and its surroundings A_∞ optically interact with each other or take place in optically active media, any considerations of radiation must take into account not only the Stefan-Boltzmann equation, but Kirchhoff's and Lambert's laws [5] as well, with which the equivalent emissivity factor $\varepsilon_{w-\infty}$ and the configuration factor $\varphi=A_w / A_\infty$ can be determined. If A_w and A_∞ are parallel, then $\varepsilon_{w-\infty}=1 / (1/\varepsilon_w + 1/\varepsilon_\infty - 1)$, and $\varphi=1$ [6]; but when A_w is inside A_∞ ($A_w << A_\infty$), then $\varepsilon_{w-\infty} \approx \varepsilon_w=\varepsilon$ [7]. Many studies have addressed various configurations of radiative heat transfer surfaces, for example [7-9].

In order to eliminate the effects of radiation in experimental

convection studies, some researchers took various approaches, performing experiments in water [10-13], glycerine [14-16] or other liquids like ethylene glycol [17], in which radiation does occur but is much smaller than convection in water (assumption Q_R=0). Others used polished copper or aluminium plates [18-21] assuming that when ε=0, Q_R is also equal to 0. The remainder calculated the radiative flux from the Stefan-Boltzmann equation for given values of ε and subtracted it from the heating power of the tested surfaces.

The following convective-radiation studies of heat transfer in a confined space are of interest: the numerical examination of the impact of solar radiation on the conversion of heat transfer from conduction to convection in a three-dimensional (3D) shallow wedge [22], and an investigation, likewise numerical, of the influence of the absorbing-emitting-scattering effect in a two-dimensional (2D) square cavity on convective-radiative heat transfer [23]. Similar problems were studied in a partitioned rectangular enclosure with semi-transparent walls [24], in a cavity with a porous horizontal layer [25], in a side open cavity [26], and also with regard to heat transfer by conduction in the study [27]. An interesting numerical study examining coupled natural convection and surface radiation through an open fracture in a solid wall facing a reservoir containing isothermal quiescent air was reported in the study [28]. A similar study of coupled free convection and radiative heat transfer in a cavity containing an isothermal vertical plate and filled with carbon dioxide or nitrogen was carried out using holographic interferometry [29]. Another numerical study using a participating medium (like carbon dioxide and water vapour) in the channel between two vertical parallel plates was reported in the study [30]. An experimental study of free convection and radiative heat transfer in air inside rectangular closed cavities of different aspect ratio with two vertical active walls (hot and cold) was described in the study [6]. The results of experimental studies of heat exchange in the channel between two symmetrically heated isothermal vertical walls using a thermal imaging camera, in which the contribution of radiation was limited by the polished surfaces of aluminium plates, were given in the studies [31, 32]. In paper [33] the relationship between radiation and convection from a vertical flat plate was interferometrically and numerically (with the FLUENT programme) investigated. The influence of its emissivity and internal heat conduction were also taken into consideration in it.

Numerical and theoretical considerations of convective-radiative heat exchange inside square and rectangular enclosures using the commercial software FLUENT 6.3 and Dimensional Analysis were given in the study [34]. The influence of radiation on laminar convective heat transfer determined in optically active media was numerically tested using the Rosseland approximation [35], and with reference to an isothermal vertical plate in the studies [36-42].

Determination of the specific heat of a vertical plate material and the emissivity of its surface with the use of transient cooling of the solid system consisting in convective-radiative cooling in the air, in the temperature range t=42 – 142°C and Ra=2·10^6 - 2·10^7, was described in papers [43, 44]. Experimental studies of convective-radiative heat transfer from a horizontal cylinder were described in the study [45] and from an isothermal vertical slender cylinder in [46], and different cases that can be found also in the studies [46-48]. The same problem, but theoretically using a similarity solution in relation to the vertical plate, was investigated and described in the studies [49-52]. The interaction of convection with radiation for a plate inclined at a small angle to the horizontal was analysed using the appropriate transformation and then solving the resulting local non-similarity equations numerically [53]. The solution of dimensionless boundary-layer equations of second-order interactions between radiation and free laminar convection from a vertical, black and isothermal plate to the surrounding grey gas was given in the studies [54, 55]. The effect of radiation on free convection was investigated experimentally in the corner formed by a horizontal plate and a vertical fin of height 30, 50 and 70 mm coated with paints of different colours to change the emissivity from 0.05 to 0.85 [56].

Clearly, there is a growing demand for research results relating, among other things, to combined convective-radiative heat exchange in construction, industry and in numerous technological problems, including internal combustion engines, furnace design, nuclear reactor safety, fluidized bed pyrolysis, heat exchangers, solar collectors and photo- and biochemical reactors. These entities are more interested in the magnitude of the heat flux supplied or emitted from a real heat exchange surface than in the heat transfer mechanisms, the participation of convection and radiation in them, the simplifying assumptions made, the experimental procedures etc. The response to this heightened interest in applications of overall convective and radiative heat transfer can be found in papers dealing with heat losses in construction [57-62] and from the housings of industrial devices (motors, pumps, exchangers) [63], and the heat fluxes transferred within specific devices, such as baking ovens [64], internal combustion engine cylinders [65] or glass furnaces [66, 67].

As mentioned above, convection and radiation have usually been considered separately. But in the case of air, they always coexist and can interact to varying extents, depending on the temperature. The proportion of heat transfer by radiation is higher than by convection and increases as the temperature of the heating surface rises. The study of the interactions of these two heat transfer mechanisms and the search for the possibility of their joint mathematical description in the form of a single empirical equation is the subject of this paper.

2. THEORETICAL BACKGROUND

2.1 Heat transfer from heated surfaces in air

The density of heat loss from a building, which is the sum of radiation and convection losses q_{C+R}, depends mainly on the temperature difference between the heat transfer surface t_w and the ambient temperature t_∞ (1). These are not only direct losses through the walls of the building, but also indirect losses through non-residential spaces (staircases, attic and cellars) as shown in the diagram in Figure 1. The mechanism of heat losses from rooms, through walls and ceiling, is connected with convective and radiative heat transfer. From the basement, on the other hand, these losses occur by conduction to the foundations and then to the ground.

Since the temperature difference ($t_{w,in}$ - t_{ground}) as well as the thermal conductivity of the foundations have small values, according to Fourier's law this heat loss flux by conduction was neglected $q_{loss,floor} \approx 0$, and further consideration was focused on the relevant convective q_C and radiative q_R partial heat loss fluxes and the total one q_{C+R} in generalized terms: for

t_w, t_∞ and the vertical surface. The obtained relations for other configurations of planar (horizontal, oblique), cylindrical or conical surfaces can be corrected by substituting the relevant C_C and n constants for these configurations in the Nusselt-Rayleigh criterion relationships (1 - 5).

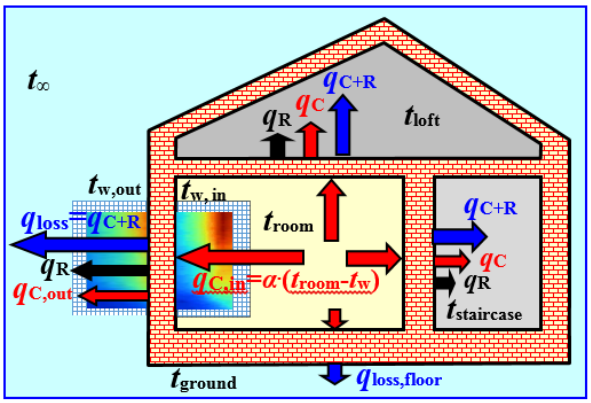

Figure 1. Types of heat loss fluxes in a model of a building with an indication of how convective heat fluxes can be directly measured, using thermal imaging camera with a grid [19, 68]

During heating or cooling in air, the temperature difference between a heated surface t_w and the surroundings t_∞ causes heat to be exchanged by convection (according to Newton's law, this is proportional to the heat transfer coefficient α_C), and by radiation (according to the Stefan-Boltzmann theory, this is proportional to the coefficient α_R). The total heat flux q_{C+R} can be written as:

$$q_{C+R} = q_C + q_R = \alpha_C \cdot \Delta t + \sigma \cdot \varepsilon \cdot (T_w^4 - T_\infty^4) = \alpha_{C+R} \cdot \Delta t \quad (1)$$

where:

$$\alpha_C = \frac{\lambda}{l} \cdot Nu_C = \frac{\lambda}{l} \cdot C_C \cdot Ra^n, \quad (2)$$

and similarly

$$\alpha_{C+R} = \frac{\lambda}{l} \cdot Nu_{C+R} = \frac{\lambda}{l} \cdot C_{C+R} \cdot Ra^n, \quad (3)$$

Substituting (2) and (3) in (1) gives:

$$\frac{\lambda}{l} \cdot C_C \cdot Ra^n + \frac{\sigma \cdot \varepsilon}{\Delta t} \cdot (T_w^4 - T_\infty^4) = \frac{\lambda}{l} \cdot C_{C+R} \cdot Ra^n, \quad (4)$$

and then

$$C_{C+R} = C_C + \frac{\sigma \cdot \varepsilon \cdot l}{\lambda \cdot \Delta t \cdot Ra^n} \cdot (T_w^4 - T_\infty^4). \quad (5)$$

Analysis of Eq. (5) suggests the following cases:

- C_C values are known from the literature, where they are given in the form of the dependence of Nusselt and Rayleigh numbers obtained from experimental, theoretical and numerical research:

$$Nu_C = C_C \cdot Ra^n. \quad (6)$$

- the value of C_{C+R} can be determined from the measured heating power q and the heat loss fluxes q_{str}, as:

$$\alpha_{C+R} \cdot \Delta t = q_{C+R} = q - q_{str}, \quad (7)$$

$$C_{C+R} = \frac{Q - Q_{loss}}{A \cdot \Delta t} = \frac{U \cdot I \cdot l}{A \cdot \lambda \cdot \Delta t \cdot Ra^n} \quad (8)$$

for electric heating with a current power $Q = U \cdot I$, heat transfer area A, characteristic linear dimension l, and when the heat flux is transferred in its entirety to the heated medium ($q_{str}=0$).

- the emissivity ε of a heated surface is known or can be determined, e.g., with a thermal imaging camera; nonetheless, its value is encumbered with a certain error [69, 70].
- any combination of the three above cases.

2.2 Vertical heated plate

Further considerations of the coexisting mechanisms of heat exchange in the air, i.e., natural convection and radiation, were carried out on the longest tested and best known configuration of the heated surface, i.e. the vertical heated plate. Until recently, the results of theoretical, experimental and numerical research obtained for this were the most frequently published in the scientific literature on free convection, so this configuration of the heated surface is the most representative for validating the correctness of the considerations discussed in this paper.

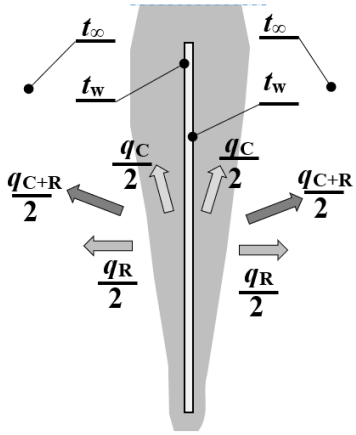

Figure 2. Draft scheme of a thin, double-sided, heated isothermal vertical plate

In the case of electric heating, the heating power can be written as $Q = U \cdot I$, and in the case of a double-sided vertical plate of width b, height h and area $A = 2 \cdot b \cdot h$, the heat energy flux q_{C+R} transferred to the environment consisting, according to Figure 2 and Eq. (1), of two convective $q_C/2$ and two radiative $q_R/2$ fluxes, is proportional to the equivalent (convective-radiative) heat transfer coefficient α_{C+R}, according to the relationship:

$$q_{C+R} = \alpha_{C+R} \cdot \Delta t = \frac{Q - Q_{loss}}{A} = \frac{U \cdot I - Q_{loss}}{A}. \quad (9)$$

Assuming for a thin, double-sided plate that the heat loss $Q_{loss}=0$ [71], the total heat transfer coefficient α_{C+R} and the Nusselt number Nu_{C+R} can be written as:

$$\alpha_{C+R} = \frac{U \cdot I}{A \cdot \Delta t} = \frac{U \cdot I}{2 \cdot b \cdot h \cdot \Delta t}, \quad (10)$$

$$Nu_{C+R} = \frac{\alpha_{C+R} \cdot h}{\lambda} = \frac{U \cdot I}{2b \cdot \lambda \cdot \Delta t}, \quad (11)$$

From the Nusselt-Rayleigh criterion dependence, analogous to (6) and (2), but for a vertical plate where n=1/4,

$$Nu_{C+R}=C_{C+R} \cdot Ra^{1/4}, \tag{12}$$

the constant C_{C+R}, described in detail by (5), can be calculated for specific temperature conditions, determined by the Rayleigh number (16):

$$C_{C+R} = \frac{Nu_{C+R}}{Ra^{1/4}}. \tag{13}$$

With the results of experimental tests, in the form of known values of t_w, t_∞, U, I, b, h for temperature conditions (Δt, t_{av}=(t_w + t_∞)/2), the physical properties of air (β, λ, ν and a), and then Nu_{C+R}, Ra and C_{C+R} can be calculated:

$$\frac{Nu_{C+R}}{Ra^{1/4}} = \frac{U \cdot I}{2b \cdot \lambda \cdot \Delta t \cdot Ra^{1/4}} = C_{C+R}. \tag{14}$$

2.2.1 The case where the heat flux is known

In industry, construction and agriculture (breeding, greenhouse crops), where the lowest possible costs of production or exploitation have to be balanced against high energy costs, technical and economic information on flux values and the amount of heat transferred in technological or operational processes is the most important. Without this information, it is hard to take responsible decisions, manage energy optimally and economically, and reduce costs.

When electrical energy is converted into thermal energy, information on the power of heating or cooling devices and the amount of heat energy they transfer can be obtained by direct measurement of the electrical heating power $Q=U \cdot I$, taking into account the efficiency of conversion, and their operation time τ. In the case of other energy carriers, e.g., heating or cooling media, to determine the amount of transferred thermal energy, the temperature drop t_{in} - t_{out} of the medium and its mass flow rate M have to be known. In the case of steam heating, the measure is the amount of condensate or the decrease in the enthalpy of the heating steam, etc.

In this situation, the value of C_{C+R} and the heat exchange mechanisms are of secondary importance to the user. Nevertheless, a knowledge of C_{C+R}, calculated from a known value of q_{C+R}, may be useful for analysing other cases of convective heat transfer in air. For this purpose, after rearranging Eq. (8), one obtains:

$$\begin{aligned} Q_{C+R} = \frac{U \cdot I}{A} = \alpha_{C+R} \cdot \Delta t = \frac{\lambda}{h} \cdot Nu_{C+R} \cdot \Delta t = \\ = \frac{\lambda}{h} \cdot C_{C+R} \cdot Ra^{\frac{1}{4}} \cdot \Delta t, \end{aligned} \tag{15}$$

$$C_{C+R} = \frac{U \cdot I \cdot h}{A \cdot \lambda \cdot \Delta t \cdot Ra^{1/4}} = \frac{U \cdot I}{2 \cdot b \cdot \lambda \cdot (T_w - T_\infty)} \cdot Ra^{-1/4}. \tag{16}$$

The values of C_{C+R} obtained for specific cases and the heating powers, temperatures, physical properties of air and Ra measured for them, can be used to determine q_{C+R} and Q_{C+R} in other heating or cooling systems, where their direct measurement is impossible. These cases are discussed in the next section.

2.2.2 The case where the heat flux and power are not known

It is not always possible to directly measure the heat flux q_{C+R} transferred by the heating medium. This applies, for example, to the heating of spaces with heat pumps, solar collectors, air heaters, as well as heat losses from buildings, cooling of electronic systems, etc. In these cases, to determine the power and amount of transferred heat, it is necessary to know the values of the coefficients C_{C+R} or C_C and C_R according to the Nusselt-Rayleigh criteria, which can be used to determine the power Q and the heat flux $q=Q/A$ transferred from the heating device to the environment.

With a known (literature) or experimentally determined value of C_{C+R}, the heat transfer flux from surface A can be calculated from (15) as follows:

$$q_{C+R} = \frac{\lambda}{h} \cdot C_{C+R} \cdot \Delta t \cdot Ra^{1/4}, \tag{17}$$

$$Q_{C+R} = q_{C+R} \cdot A = 2 \cdot b \cdot \lambda \cdot C_{C+R} \cdot \Delta t \cdot Ra^{1/4}. \tag{18}$$

If the heated or cooled object consists not only of a single double-sided heated vertical plate, but also of i- such plates or vertical pipes with a diameter d, then the area should be appropriately corrected in formula (18). $A=2 \cdot b \cdot h \cdot i$ or $A=2 \cdot \pi \cdot d \cdot h \cdot i$ should be substituted for $A=2 \cdot b \cdot h$, and if such an object contains horizontal components, e.g., a horizontal plate, cuboid or pipe, then the appropriate characteristic linear dimension l and exponent n for Ra should be used in addition.

The value of C_{C+R} can also be determined from Eq. (5), if one knows the literature values of the convective coefficient C_C and the calculated radiative heat flux.

The coefficient C_C for an isothermal vertical plate has historically taken the following example values: $C_C=Nu/Ra^{1/4}$=0.571 [72],=0.560 [73],=0.540 [74]. In the paper [75] a total of 25 plates of this type were analysed, giving an average value of $C_{C,av}=Nu/Ra^{0.252}$=0.550. This value, however, is based on the unusual exponent n for a vertical plate that is inconvenient to use, especially when comparing the results. In [71], the coefficients C_C and n in the Nusselt-Rayleigh relationship were converted for the assumed values of Ra=$10^{6, 7, 8, 9}$ from n=0.252 to n=0.250, and the following new relationships were obtained:

$$\begin{aligned} Nu_{C,av} = 0.550 \cdot Ra^{0.252}, = 0.565 \cdot Ra^{0.25} \, (Ra = 10^6), \\ = 0.573 \cdot Ra^{0.25} \, (Ra = 10^9) \end{aligned} \tag{19}$$

$$Nu_C = 0.569 \cdot Ra^{0.25} \, (Ra = 10^6 - 10^9) \text{ [71]} \tag{20}$$

This dependence differs from that given in the study [52] (C_C=0.555) by only 2.5% and is therefore used later in this paper.

Knowledge of the second part of Eq. (5), i.e., the radiative heat flux, requires the emissivity of the radiator surface ε to be known or measured in addition to the temperatures T_w and T_∞. Taking into account both components of the heat flux (convection and radiation), the following relationship can be obtained:

$$C_{C+R} = 0.569 + \frac{\sigma \cdot \varepsilon \cdot l}{\lambda \cdot \Delta t \cdot Ra^n} \cdot (T_w^4 - T_\infty^4) \tag{21}$$

In technical issues, the most important thing is to know the values of α_{C+R} and the heat transfer flux q_{C+R}, which can be calculated from Eq. (21) based on Eqns. (2), (3) and (4):

$$\alpha_{C+R} = \frac{\lambda}{l} \cdot 0.569 \cdot Ra^{\frac{1}{4}} + \frac{\sigma \cdot \varepsilon}{\Delta t} \cdot (T_w^4 - T_\infty^4) \tag{22}$$

$$\begin{aligned} q_{C+R} = \alpha_{C+R} \cdot \Delta t = \frac{\lambda}{l} \cdot 0.569 \cdot \Delta t \cdot Ra^{\frac{1}{4}} + \\ + \sigma \cdot \varepsilon \cdot (T_w^4 - T_\infty^4). \end{aligned} \tag{23}$$

3. CALCULATION STUDIES

3.1 Simulation calculations C_{C+R}=f(t_w, Δt, l, ε)

Simulation calculations, as well as theoretical, numerical and experimental considerations, require the knowledge or assumption of the temperatures of the heated surface (t_w, T_w=t_w+273.15), the undisturbed area (t_∞, T_∞=t_∞+273.15), the difference between them Δt=ΔT=t_w –t_∞ and the average air temperature T_{av}=(T_w+T_∞)/2, for which its physical properties a, c_p, β, λ, μ, ρ, ν should be determined. These properties are now available online; in the past, they had to be read from tables, such as [1, 76].

3.1.1 Calculation of the physical properties of air

For the purposes of this work, based on the study [77], the following formulas were derived for calculating the physical properties of air for a given temperature T_{av} in the range 120 ≤ T_{av} ≤ 480 K [77]:

$$\beta = 1/T_{av}\ [1/K],\ \text{or}\ \beta = 7.17643\cdot10^{-13}\cdot T_{av}^4 - 2.76969\cdot10^{-10}\cdot T_{av}^3 + 5.36690\cdot10^{-8}\cdot T_{av}^2 - 1.29663\cdot10^{-5}\cdot T_{av} + 3.65078\cdot10^{-3}\ [1/K],\quad R^2=0.9998, \tag{24}$$

$$a = -7.76593\cdot10^{-14}\cdot T_{av}^3 + 1.10718\cdot10^{-10}\cdot T_{av}^2 + 8.70331\cdot10^{-8}\cdot T_{av} + 1.3323\cdot10^{-5}\ [m^2/s],\quad R^2=0.9999, \tag{25}$$

$$\nu = -1.60765\cdot10^{-13}\cdot T_{av}^3 + 1.77128\cdot10^{-10}\cdot T_{av}^2 + 1.25673\cdot10^{-7}\cdot T_{av} + 1.85135\cdot10^{-5}\ [m^2/s],\quad R^2=0.9999, \tag{26}$$

$$\lambda = 3.13755\cdot10^{-11}\cdot T_{av}^3 - 4.27648\cdot10^{-8}\cdot T_{av}^2 + 7.70091\cdot10^{-5}\cdot T_{av} + 2.4048\cdot10^{-2}\ [W/(m\cdot K)],\quad R^2=0.9999. \tag{27}$$

In order to perform simulation calculations of heat transfer in air, the following values were assumed: heated surface temperatures t_w=90, 80, 70, 60, 50, 40, 30 and 20°C and the temperature difference Δt=t_w – t_∞=5, 10, 15, 20, 40 and 60 K, the combination of which determined the temperature of the undisturbed area t_∞ and the average air temperature t_{av}=(t_w + t_∞)/2.

3.1.2 Introduction of thermodynamic and thermo-emission functions

By introducing the function $B1$, which determines the thermodynamic properties of air, and $B2$, related to its thermo-emission, Eq. (21) can be converted into the form:

$$C_{C+R} = C_C + C_R = C_C + \frac{\sigma\cdot\varepsilon\cdot l\cdot(T_w^4 - T_\infty^4)}{\lambda\cdot(T_w - T_\infty)\cdot Ra^{1/4}} = C_C + B1\cdot B2\cdot l^{1/4}\cdot\varepsilon, \tag{28}$$

where:

$$B1 = \frac{1}{\lambda\cdot\left(\frac{g\cdot\beta\cdot\Delta t}{\nu\cdot a}\right)^{\frac{1}{4}}},\ m^{7/4}\cdot K/W, \tag{29}$$

$$B2 = \frac{\sigma\cdot(T_w^4 - T_\infty^4)}{\Delta t},\ W/(m^2K), \tag{30}$$

$$Ra = \left(\frac{l^{3/4}}{\lambda\cdot B1}\right)^4 = \frac{g\cdot\beta\cdot\Delta t\cdot l^3}{\nu\cdot a}. \tag{31}$$

Convective heat transfer, especially in fluids not accompanied by radiation, is more difficult to study experimentally, but it is easier to understand and obtain reliable and reproducible results in the form of C_C=Nu/Ra^n. It is simpler to conduct research in air, especially when a surface is heated electrically, but the inconclusive influence of radiation complicates the interpretation of the results. Perhaps by determining the effect of temperature, separately on the functions $B1$ and $B2$ and on their product $B1\cdot B2$, it will be easier to describe convective-radiative heat transfer and obtain more reliable results.

The measurement uncertainties of the values taken from table data [1, 71, 76-78], was assumed at the level of the last significant digit in the data source. For a temperature measurement the accuracy of ±0.1°C was assumed, but for the temperature differences, according with the study [71], the calculations permit an accuracy of ±0.05 K to be specified. The maximum relative uncertainties of Ra and C_{C+R}, derived from Eqns. (31) and (21) are: δRa_{max}=± 4.7% and $\delta C_{C+R\ max}$=± 8.5%. In order to preserve the clarity of the presentation the uncertainty of measurement in relation to the maximum relative uncertainty δC_{max} are only be given in the following investigation. A detailed analysis of the measurement uncertainties related to this consideration can be found in ref. [71].

Table 1. Calculated values of $B1$ and $B2$ for given values of t_w, t_∞ and l

Temperatures				Physical properties of air				$B1$ (Figure 3.a)		$B2$ (Figure 3.b)		$B1\cdot B2$ (Figure 4)		
t_w	t_∞	t_{av}	Δt	$\lambda\cdot10^{-2}$	$\beta\cdot10^{-3}$	$a\cdot10^{-5}$	$\nu\cdot10^{-5}$	(29)	(35)	(30)	(33)	(34)	(35)	(36)
°C	°C	°C	K	W/m·K	1/K	m²/s	m²/s	$m^{7/4}K/W$		$W/(m^2K)$		$1/m^{1/4}$		
90	85	87.5	5	3.0439	2.7843	3.0758	2.1734	0.2748	0.2768	10.640	10.7426	2.9239	2.9735	2.9779
80	75	77.5	5	2.9746	2.8656	2.9242	2.0697	0.2723	0.2744	9.7797	9.7945	2.6632	2.6875	2.6923
70	65	67.5	5	2.9042	2.9501	2.7754	1.9678	0.2699	0.2720	8.9667	8.9302	2.4199	2.4287	2.4341
60	55	57.5	5	2.8330	3.0380	2.6295	1.8679	0.2675	0.2696	8.2000	8.1421	2.1931	2.1948	2.2007
50	45	47.5	5	2.7607	3.1300	2.4865	1.7699	0.2650	0.2671	7.4783	7.4236	1.9820	1.9832	1.9896
40	35	37.5	5	2.6875	3.2269	2.3467	1.6738	0.2626	0.2647	6.8002	6.7684	1.7859	1.7918	1.7988
30	25	27.5	5	2.6134	3.3295	2.2100	1.5799	0.2602	0.2623	6.1645	6.1711	1.6039	1.6188	1.6263
20	15	17.5	5	2.5383	3.4389	2.0766	1.4880	0.2577	0.2599	5.5696	5.6265	1.4355	1.4623	1.4703
90	80	85.0	10	3.0266	2.8043	3.0377	2.1473	0.2306	0.2306	10.422	10.5274	2.4028	2.4277	2.3834
80	70	75.0	10	2.9571	2.8864	2.8867	2.0441	0.2285	0.2286	9.5735	9.5915	2.1873	2.1922	2.1533
70	60	65.0	10	2.8865	2.9717	2.7386	1.9427	0.2264	0.2265	8.7721	8.7389	1.9863	1.9793	1.9454
60	50	55.0	10	2.8150	3.0606	2.5935	1.8432	0.2244	0.2244	8.0168	7.9620	1.7989	1.7870	1.7576
50	40	45.0	10	2.7425	3.1538	2.4513	1.7457	0.2224	0.2224	7.3061	7.2542	1.6246	1.6132	1.5879

40	30	35.0	10	2.6690	3.2519	2.3122	1.6501	0.2203	0.2203	6.6387	6.6094	1.4627	1.4563	1.4346
30	20	25.0	10	2.5947	3.3561	2.1764	1.5567	0.2183	0.2183	6.0132	6.0218	1.3126	1.3144	1.2960
20	10	15.0	10	2.5194	3.4675	2.0438	1.4653	0.2162	0.2162	5.4284	5.4865	1.1736	1.1863	1.1709
90	75	82.5	15	3.0093	2.8246	2.9997	2.1213	0.2079	0.2073	10.208	10.3090	2.1218	2.1366	2.0981
80	65	72.5	15	2.9395	2.9074	2.8495	2.0185	0.2060	0.2054	9.3712	9.3859	1.9304	1.9277	1.8941
70	55	62.5	15	2.8687	2.9936	2.7021	1.9176	0.2041	0.2035	8.5814	8.5455	1.7518	1.7391	1.7100
60	45	52.5	15	2.7969	3.0835	2.5576	1.8186	0.2023	0.2016	7.8373	7.7803	1.5855	1.5688	1.5438
50	35	42.5	15	2.7242	3.1778	2.4162	1.7216	0.2005	0.1998	7.1375	7.0836	1.4308	1.4151	1.3937
40	25	32.5	15	2.6505	3.2774	2.2779	1.6266	0.1986	0.1979	6.4806	6.4493	1.2872	1.2763	1.2582
30	15	22.5	15	2.5760	3.3832	2.1429	1.5336	0.1968	0.1960	5.8654	5.8719	1.1541	1.1510	1.1359
20	5	12.5	15	2.5005	3.4966	2.0112	1.4428	0.1949	0.1942	5.2903	5.3461	1.0310	1.0380	1.0255
The average discrepancy over the entire tested range of Δ*t* (5–30 K) in relation to (34)												100%	99.63%	99.62%

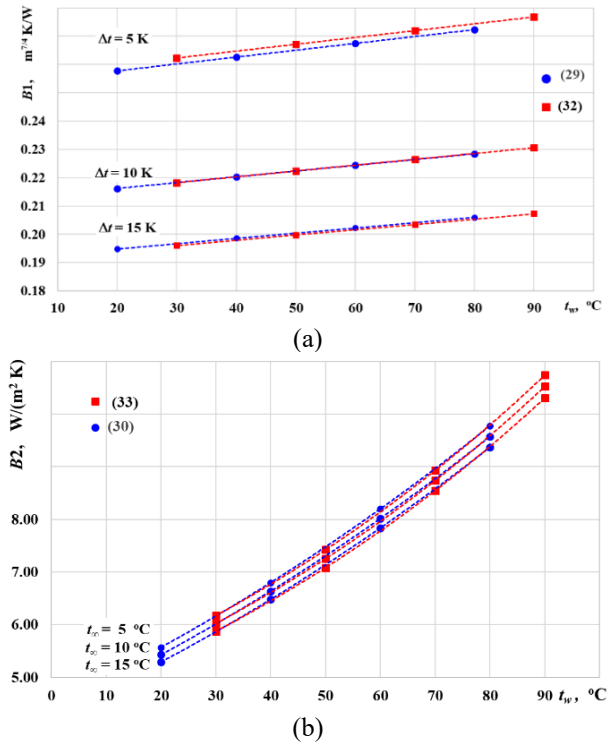

Figure 3. Values of *B*1 calculated from Eqns. (29) and (32) for Δ*t*=5, 10 and 15 K as a function of the heating surface temperature varying in the range t_w=20 – 90°C (a) compared with values of *B*2 calculated from Eqns. (30) and (33) for t_∞= 5, 10 and 15 K (Δ*t*=t_w – t_∞) as a function of the heating surface temperature varying in the range t_w=20 – 90°C (b)

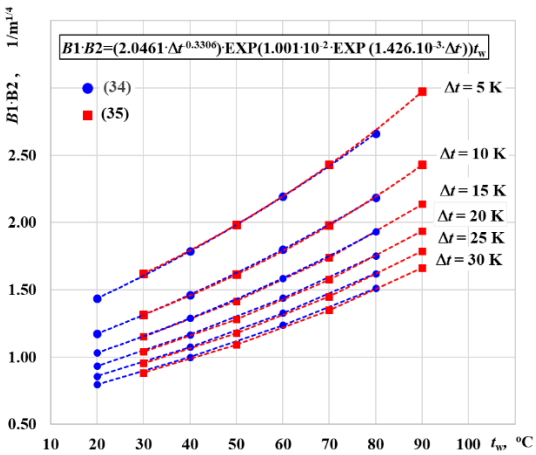

Figure 4. Comparison of values of *B*1·*B*2 calculated from Eqns. (34) (blue circles) and (35) (red squares). Eq. (36), shown in the box, is the result of the approximation of the curves obtained using Eq. (34)

3.1.3 Investigation of the influence of t_w and Δ*t* on the values of *B*1 and *B*2

Having determined t_∞ and t_{av} and the thermodynamic properties of air for given values of t_w=90, 80, 70, 60, 50, 40, 30 and 20°C, together with Δ*t*=5, 10, 15, 20, 40 and 60 K, the values of *B*1, *B*2 and their product were calculated. Some of the results of these simulation calculations, for Δ*t*=5, 10 and 15 K, are summarized in Table 1 and Figure 3.

From the variability of *B*1 (29) and *B*2 (30) in the temperature range t_w=0 – 90°C for the set Δ*t*=5, 10, 15, 20, 25 and 30 K, and the resulting values of t_∞, t_{av}, the following approximation relationships were determined:

$$B1 = 3.503 \cdot 10^{-4} \cdot \Delta t^{-0.2315} \cdot t_w + 0.3914 \cdot \Delta t^{-0.2661}, \quad (32)$$

$$B2 = (-2.457 \cdot 10^{-2} \Delta t + 4.800) \cdot e^{(1.418 \cdot 10^{-5} \cdot \Delta t + 9.168 \cdot 10^{-3}) \cdot t_w}, \quad (33)$$

The calculated values of *B*1 from (29) and (32), and *B*2 from (30) and B2 (33) are compared graphically in Figure 3, in which, as in Table 1, the presentation is limited only to example values obtained for the range t_w=20 – 90°C, and Δ*t*=5, 10 and 15 K.

Apart from the values of *B*1 and *B*2, on the basis of which relationships (32) and (33) were derived, the values of their product *B*1·*B*2 were also calculated (see Table 1). To calculate them, the formulas obtained from the conversions of (29) and (30) as well as (32) and (33) to (34) and (35) were used:

$$B1 \cdot B2 = \frac{1}{\lambda \cdot \left(\frac{g \cdot \beta \cdot \Delta t}{\nu \cdot a}\right)^{\frac{1}{4}}} \cdot \frac{\sigma \cdot (T_w^4 - T_\infty^4)}{\Delta t}, \quad (34)$$

$$B1 \cdot B2 = (3.503 \cdot 10^{-4} \cdot \Delta t^{-0.2315} \cdot t_w + 0.3914 \cdot \Delta t^{-0.2661}) \cdot (-2.457 \cdot 10^{-2} \Delta t + 4.800) \cdot e^{(1.418 \cdot 10^{-5} \cdot \Delta t + 9.168 \cdot 10^{-3}) \cdot t_w}. \quad (35)$$

The values of *B*1·*B*2 calculated from these formulas are given in the relevant columns of Table 1 and in Figure 4. Note that Table 1 lists only results obtained for Δ*t*=5, 10 and 15 K, whereas Figure 4 contains all the curves for *B*1·*B*2 (t_w, Δ*t*). The curves marked with blue lines and circles are a graphic representation of Eq. (34), those with red lines and squares represent Eq. (35).

As a result of the approximations of the *B*1·*B*2 (t_w) curves shown in Figure 4, obtained on the basis of equation (34) (blue circles and lines) for Δ*t*=5, 10, 15, 20, 25 and 30 K, one universal relationship was obtained:

$$B1 \cdot B2 = (2.0461 \cdot \Delta t^{-0.3306}) \cdot e^{\left(1.008 \cdot 10^{-2} \cdot e^{1.426 \cdot 10^{-3} \cdot \Delta t}\right) \cdot t_w}, \quad (36)$$

The results of the calculations for given t_w and Δt obtained with the aid of this universal relationship are listed in the last column of Table 1. Like those resulting from the previous approximation (35), they exhibit a slight (only 0.37 and 0.38%) average discrepancy in relation to the results obtained using the original Eq. (34). This discrepancy concerns the entire scope of the calculations, only partially visualized in Table 1.

3.1.4 Analysis of the influence of t_w and Δt on C_R values

The dependence on the radiative constant in the Nusselt-Rayleigh criterion relationship C_R can be obtained by substituting into (28) one of three equivalent formulas for $B1 \cdot B2$: (34), (35) or (36). In the case of substitution (36) one obtains:

$$C_R = B1 \cdot B2 \cdot l^{\frac{1}{4}} \cdot \varepsilon = (2.0461 \cdot \Delta t^{-0.3306}) \cdot e^{\left(1.008 \cdot 10^{-2} \cdot e^{1.426 \cdot 10^{-3} \cdot \Delta t}\right) \cdot t_w} \cdot l^{1/4} \cdot \varepsilon, \quad (37)$$

The linear influence of the surface emissivity factor ε on C_R, being obvious and predictable (C_R=0 for ε=0 and C_R=$C_{R,max}$ for ε=1); hence, by assuming ε=1.0, it was omitted at this stage of the calculations. In contrast, analysis of the influence of the characteristic linear dimension l on C_R cannot be omitted, because through $B1$ (31) it influences the value of the Rayleigh number, by means of which the intensity of convective heat exchange is described. While it is customary in convection that $C_C \neq f(Ra)$=const, it does not also have to apply to radiative heat transfer, for which it has been neither tested nor proven.

Table 2 shows the values of C_R and Ra obtained from relationship (37) for given values of the surface temperature t_w=100, 90, 80, 70, 60, 50, 40, 30, 25, 20 and 15°C, three values of the undisturbed area temperature t_∞=10, 5 and 0°C, the constant value of the emissivity coefficient ε=1.0, and the following values of the characteristic linear dimension l=0.5, 0.25, 0.15, 0.10, 0.05 and 0.01 m. The values of Ra given in the Table 2 were calculated, as in Table 1, using relationships (14 - 27) as a function of t_{av}, but in order to keep Table 2 readable, it does not include the calculated values of a, β and ν.

Table 2. Results of C_R and Ra calculations for given values of t_w, t_∞ and l and the assumed constant value of ε=1

Temp.		$B1 \cdot B2$	l=0.50 m		l=0.25 m		l=0.15 m		l=0.10 m		l=0.05 m		l=0.01 m	
t_w	t_∞	(36)	C_R (37)	$Ra \cdot 10^{-10}$	C_R (37)	$Ra \cdot 10^{-9}$	C_R (37)	$Ra \cdot 10^{-8}$	C_R (37)	$Ra \cdot 10^{-8}$	C_R (37)	$Ra \cdot 10^{-7}$	C_R (37)	$Ra \cdot 10^{-5}$
°C	°C	$1/m^{1/4}$	–	–	–	–	–	–	–	–	–	–	–	–
100	0	1.4161	1.1908	2.7625	1.0013	3.4531	0.8813	7.4588	0.7963	2.2100	0.6696	2.7625	0.4478	2.2100
90	0	1.2873	1.0825	2.6291	0.9103	3.2863	0.8011	7.0984	0.7239	2.1032	0.6087	2.6291	0.4071	2.1032
80	0	1.1792	0.9916	2.4736	0.8338	3.0920	0.7338	6.6787	0.6631	1.9789	0.5576	2.4736	0.3729	1.9789
70	0	1.0894	0.9161	2.2933	0.7703	2.8666	0.6780	6.1919	0.6126	1.8346	0.5152	2.2933	0.3445	1.8346
60	0	1.0167	0.8550	2.0849	0.7189	2.6061	0.6327	5.6293	0.5718	1.6679	0.4808	2.0849	0.3215	1.6679
50	0	0.9609	0.8080	1.8448	0.6795	2.3060	0.5980	4.9810	0.5404	1.4758	0.4544	1.8448	0.3039	1.4758
40	0	0.9234	0.7765	1.5688	0.6529	1.9610	0.5747	4.2358	0.5193	1.2551	0.4366	1.5688	0.2920	1.2551
30	0	0.9093	0.7646	1.2522	0.6430	1.5652	0.5659	3.3809	0.5113	1.0017	0.4300	1.2522	0.2875	1.0017
25	0	0.9149	0.7694	1.0769	0.6470	1.3462	0.5694	2.9077	0.5145	0.8616	0.4327	1.0769	0.2893	0.8616
20	0	0.9338	0.7853	0.8895	0.6603	1.1118	0.5812	2.4015	0.5251	0.7116	0.4416	0.8895	0.2953	0.7116
15	0	0.9744	0.8194	0.6889	0.6890	0.8611	0.6064	1.8600	0.5479	0.5511	0.4608	0.6889	0.3081	0.5511
100	5	1.4285	1.2012	2.5530	1.0101	3.1913	0.8890	6.8932	0.8033	2.0424	0.6755	2.5530	0.4517	2.0424
90	5	1.3024	1.0952	2.4143	0.9209	3.0179	0.8105	6.5187	0.7324	1.9315	0.6159	2.4143	0.4118	1.9315
80	5	1.1969	1.0065	2.2537	0.8464	2.8172	0.7449	6.0851	0.6731	1.8030	0.5660	2.2537	0.3785	1.8030
70	5	1.1103	0.9337	2.0685	0.7851	2.5856	0.6910	5.5850	0.6244	1.6548	0.5250	2.0685	0.3511	1.6548
60	5	1.0416	0.8758	1.8555	0.7365	2.3193	0.6482	5.0098	0.5857	1.4844	0.4925	1.8555	0.3294	1.4844
50	5	0.9912	0.8335	1.6111	0.7009	2.0138	0.6168	4.3499	0.5574	1.2888	0.4687	1.6111	0.3134	1.2888
40	5	0.9622	0.8091	1.3312	0.6804	1.6640	0.5988	3.5943	0.5411	1.0650	0.4550	1.3312	0.3043	1.0650
30	5	0.9637	0.8103	1.0114	0.6814	1.2642	0.5997	2.7307	0.5419	0.8091	0.4557	1.0114	0.3047	0.8091
25	5	0.9832	0.8268	0.8348	0.6952	1.0435	0.6119	2.2539	0.5529	0.6678	0.4649	0.8348	0.3109	0.6678
20	5	1.0255	0.8623	0.6462	0.7251	0.8077	0.6382	1.7446	0.5767	0.5169	0.4849	0.6462	0.3243	0.5169
15	5	1.1129	0.9359	0.4447	0.7870	0.5559	0.6926	1.2008	0.6259	0.3558	0.5263	0.4447	0.3519	0.3558
100	**10**	**1.4425**	**1.2130**	**2.3535**	**1.0200**	**2.9418**	**0.8977**	**6.3543**	**0.8112**	**1.8828**	**0.6821**	**2.3535**	**0.4562**	**1.8828**
90	10	1.3192	1.1093	2.2100	0.9328	2.7625	0.8210	5.9670	0.7418	1.7680	0.6238	2.2100	0.4172	1.7680
80	10	1.2168	1.0232	2.0448	0.8604	2.5560	0.7573	5.5210	0.6843	1.6359	0.5754	2.0448	0.3848	1.6359
70	10	1.1339	0.9535	1.8552	0.8018	2.3190	0.7056	5.0090	0.6376	1.4842	0.5362	1.8552	0.3586	1.4842
60	10	1.0699	0.8997	1.6381	0.7566	2.0476	0.6659	4.4228	0.6017	1.3104	0.5059	1.6381	0.3383	1.3104
50	10	1.0266	0.8633	1.3899	0.7259	1.7374	0.6389	3.7528	0.5773	1.1120	0.4855	1.3899	0.3246	1.1120
40	**10**	**1.0094**	**0.8488**	**1.1069**	**0.7138**	**1.3836**	**0.6282**	**2.9886**	**0.5677**	**0.8855**	**0.4773**	**1.1069**	**0.3192**	**0.8855**
30	10	1.0351	0.8704	0.7844	0.7320	0.9805	0.6442	2.1179	0.5821	0.6275	0.4895	0.7844	0.3273	0.6275
25	10	1.0793	0.9076	0.6068	0.7632	0.7585	0.6717	1.6384	0.6069	0.4855	0.5104	0.6068	0.3413	0.4855
20	10	1.1709	0.9846	0.4174	0.8280	0.5217	0.7287	1.1270	0.6584	0.3339	0.5537	0.4174	0.3703	0.3339
15	**10**	**1.3981**	**1.1756**	**0.2154**	**0.9886**	**0.2692**	**0.8701**	**0.5815**	**0.7862**	**0.1723**	**0.6611**	**0.2154**	**0.4421**	**0.1723**

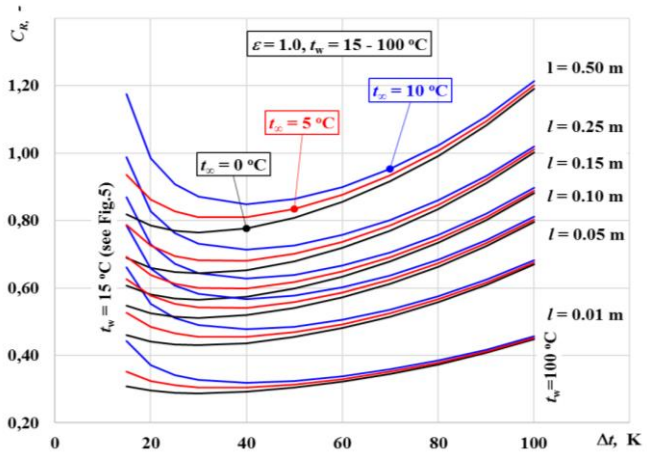

Figure 5. Graphical interpretation of the influence of t_w, t_∞, and l on C_R expressed by the function C_R=f(Δt) assuming ε=1 in relationship (37)

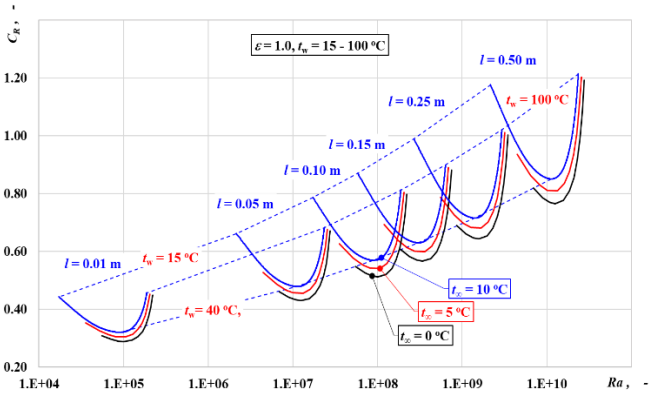

Figure 6. The influence of t_w, t_∞, and l on C_R, calculated from the dependence (37) assuming ε =1, expressed in the form of the function C_R=f(Ra)

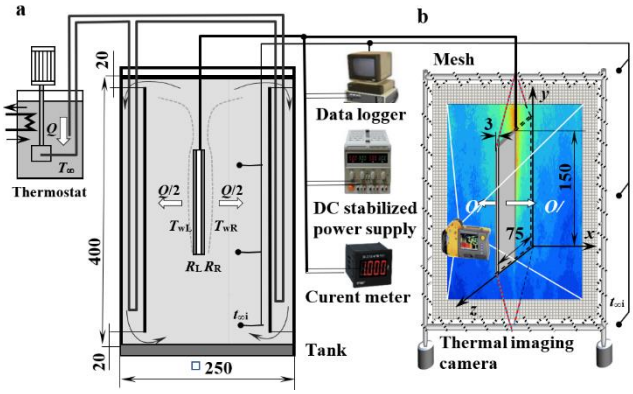

Figure 7. Diagram of the experimental apparatus for examining: a) free convective heat transfer in water, using the balance method and an isothermal vertical plate, b) total convective and radiative heat transfer in air, obtained by the use of balance method, and the convective only, obtained by the gradient method, with the additional use of IR camera with detection mesh [71]

From among the various possible graphical presentations of the results in Table 2, it was decided to show the relationships C_R=f(Δt) in Figure 5 and C_R=f(Ra) in Figure 6. In both figures the results for the same temperature of the undisturbed area are indicated for t_∞=10°C by a blue line, for t_∞=5°C by a red one, and for t_∞=0°C by a black one. In Figure 5, the beginnings of the curves related to the heated surface temperature t_w=15°C are on the left side of the graph, those for t_w=100°C on the right. Because these positions are correlated with the values of Δt, they are easier to analyse. In the case of Figure 6, where there is no such correlation, the two outermost dashed blue lines connecting the points with the highest and lowest surface temperatures t_w=15 and 100°C and a third line of minimum C_R values for $t_w \approx$ 40°C have been added, but only for t_∞=10°C these lines were created on the basis of the data shown in bold in Table 2.

Figures 5 and 6 show that the function C_R in radiative heat exchange is not constant, as was the case with C_C, which was correct for convective heat exchange. The function C_R defined in this way depends on the coefficient C_R of the emissivity ε, the temperature conditions t_w and t_∞, the area of the heated surface l, which determine the Rayleigh number, but also on the thermodynamic properties of air a, β and ν, which are included in Ra.

3.1.5 Final solution in the form of C_{C+R} and its application

Knowing the convective constant C_C and the radiative function C_R, described by Eq. (37), one can determine the value of C_{C+R}=C_C+C_R from Eq. (28) depending on the criterion dependence (12), which in turn opens up the possibility of determining the total (convective-radiative) heat flux Q_{C+R} from any vertical surface:

$$C_{C+R} = C_C + B1 \cdot B2 \cdot l^{\frac{1}{4}} \cdot \varepsilon = \frac{Nu_{C+R}}{Ra^{\frac{1}{4}}} = \frac{\alpha_{C+R} \cdot l}{\lambda \cdot Ra^{1/4}}, \quad (38)$$

$$Q_{C+R} = \frac{\lambda \cdot A}{l} \cdot \Delta t \cdot Ra^{1/4} \cdot \left(C_C + B1 \cdot B2 \cdot l^{\frac{1}{4}} \cdot \varepsilon\right). \quad (39)$$

At first glance, these equations seem complicated and require more time to obtain the results than existing solutions. However, their advantage is that, after measuring t_w, t_∞ and ε, one can use a thermal imaging camera with appropriate software to directly determine the heat flux from any heated surface of known dimensions l, e.g., a building surface. For this purpose, Eqns. (20), (24)-(27), (31), (37), (39) should only include Δt, t_{av}, ε and l, along with the literature value of the constant of free convection from a vertical plate, e.g., C_C=0.569 [71]. In the case of horizontal surfaces, this constant and the exponent n will have different values depending on criterion (2) and hence, the entire solution.

In this solution, the heat exchange is assumed by default to be in the laminar range, i.e. from $Ra_{cr,I} \approx 10^3$ to $Ra_{cr,II} \approx 10^9$ ($Ra_{cr,air}$=2.0·10^8 and $Ra_{cr,water}$=3.4·10^9 [79] for uniform flux) because above and below this range, heat transfer takes place by conduction or transition convection; for the latter, there are other values of the constants in Nusselt-Rayleigh criterion dependence (6) and (20), e.g. C_C=0.135 and n=1/3.

4. RESULTS DISCUSSION

4.1 Experimental validation of the solution

At the very beginning of this section, it should be noted that the titular validation concerns only the correctness of the solution for the constant C_{C+R} depending on Nu=C_{C+R}·$Ra^{1/4}$, describing convective-radiative heat transfer. The tests of convective heat transfer in water obtained by the use of the

balance method (a) and convective heat transfer in air obtained by the gradient method with the use of thermal imaging camera with a detection mesh, as well as combined convective and radiative heat transfer in air obtained by the use of balance method without a camera and mesh (b) were carried out on the test stand shown diagrammatically in Figure 7. Since the details of these studies have already been described in the study [71], they have been omitted here, except for the results. Based on an analysis of the relationships between the measured values of C_C, $B_1 \cdot B_2$ and C_{C+}, these results were used to develop an empirical relationship (39) and to verify it experimentally. On the test stand shown in Figure 7a, the balance method was used to determine the value of $C_{C,water}$=0.536 for an isothermal vertical plate and free convection in water, while on the test stand illustrated in Figure 6b, the new gradient method of detecting convection with a thermal imaging camera equipped with a detecting mesh was used to determine the value of $C_{C,air}$=0.579 for air [71]. On the same test stand, but using the balance method, the constant value of C_{C+R}=1.220 was obtained for air, which covers both convection and radiation heat transfer [71].

4.1.1 Research test stand

The main element of the above test stands was a thin double-sided and symmetrically heated vertical plate of height h=0.15 m, width b=0.075 m and thickness s=0.003 m. The plate was made from three layers of copper-laminated glass-epoxy composite, each 0.6 mm thick. The outer layers (LAM100X160E0.6), laminated on one side with a copper layer of thickness g=35 μm, consisted of two surface resistance thermometers with resistances 235.1 Ω and 240.7 Ω, located on both sides of the plate. The middle layer (LAM100X160ED0.6), laminated on both sides with 18 μm thick copper layers, was a two-sided heating resistance heater with 44.8 Ω and 45.2 Ω resistances, which was powered by two power supplies with power N=30 W, voltage U=0 - 10 V and current I=0 - 3 A.

Both thermometers and heaters were made by etching the resistance paths in copper by photolithography. More information, including dimensions, drawings and photos, on the production and calibration of the heater used in these tests can be found in the study [71]. A similar concept of a double-sided isothermal plate set obliquely was used in the study [80].

4.1.2 The study of radiative-convective heat transfer in air

The convective-radiative heat transfer study was carried out in the traditional way, by gradually increasing the heating power of the heaters. Since the heat exchange was symmetrical, as evidenced by practically the same surface temperatures on both sides of the plate, the heater was connected in series. After establishing the thermodynamic equilibrium t_w, t_{av} and Δt, the result was recorded, the power increased and another measurement started.

The results of the voltage and direct current variation of the heater I_i, A, U_i, V, obtained in tabular form, enabled the heat flux Q_i transferred to the air from the N_i power to be calculated. It was decided not to take into account the heat loss flux at the edges owing to the small surface area (thickness s=3 mm).

Then, based on the values of λ_i=f(t_{av}) obtained from (27) and the dimension b=0.075 m of the plate, Nu_i was calculated from Eq. (11).

In turn, knowing the temperatures of both sides of the plate surface $t_{wI,i}$ and $t_{wII,i}$ and the air in the undisturbed area $t_{\infty,i}$, the average temperatures of the plate surface and air $t_{w,i}$, $t_{av,i}$ and Δt_i could be calculated, from which the physical properties of the air could be determined from (24), (25) and (26) and consequently, the Rayleigh numbers for h=0.15 m and Δt_i from Eq. (31).

The last procedure for processing the experimental data was to calculate the individual values of $C_{C+R}=Nu_{C+R}/Ra^{1/4}$, some of which (diamonds in Figure 6) along with the mean are given in the experimental part of Table 3. The last row of Table 3 shows the averages of the results of all the research, both experimental and theoretical.

Paper [71] gives identical results, obtained on the same stand for air, but the content of Table 3 has changed. This shows the results of convective transfer, not tabulated in the study [71], and thus the differences in averaging the tabular data. On the other hand, the difference in averaging all the results $C_{C+R,av}$=1.197 (maximum relative uncertainty $\delta C_{exp.}$= 8.5%) differs slightly from that given in the study [71]. $C_{C+R,av}$=1.220 results from the use of other formulas to determine the physical properties of air in both papers. The present Eqns. (24) - (27) are correlated with t_{av} and the previous ones with other constants from T_{av}.

In the study [71], apart from the convective-radiative heat transfer in air, tests of free convection in water, in which radiative heat transfer can be omitted, were carried out on a different stand (see Figure 7a), but with the same heating plate. The criterion dependence obtained in those studies for water takes the following form:

$$Nu_C=(0.536 \pm 0.073) \cdot Ra^{0.25} \, (Ra = 2 \cdot 10^6 - 8 \cdot 10^8), \qquad (40)$$

This dependence is 5.8% less than (20), but because it was obtained as a result of experimental studies carried out in a similar way and on the same heating plate, we decided to use it to validate the correctness of the solution. Detailed calculations of this validation can be found in the study [78]. The maximum relative uncertainty $\delta C_{exp.}$=±13.7% (for the experiment conducted in water) has been included in Eq. (40).

Table 3 also lists the results obtained from processing the experimental data using equations derived from theoretical considerations. The values of function $B1 \cdot B2$, given in the theoretical part of Table 3, were based on Eq. (36), in which the experimental values of t_w and Δt were substituted.

Table 3. Results of overall (convective and radiative) heat transfer tests from a vertical plate in air

Heating power N	**Temperature**				**Experimental results**			**Comparison with theory**				
					Nu_{C+R}	**$Ra \cdot 10^{-6}$**	**C_{C+R}**	**$B1 \cdot B2$**	**C_R**	**C_{C+R}**	**C_R**	**C_{C+R}**
									ε=0.884		**ε=0.932**	
	t_w	**t_∞**	**t_{av}**	**Δt**	**(11)**	**(31)**	**(13)**	**(36)**	**(37)**	**(41)**	**(37)**	**(41)**
W	°C	°C	°C	K	-	-	-	$m^{-1/4}$	-	-	-	-
Series I												
1.0	28.5	23.9	26.2	4.6	53.207	1.496	1.521	1.642	0.903	1.439	0.952	1.488
1.8	32.8	24.1	28.4	8.7	53.372	2.700	1.317	1.396	0.768	1.304	0.810	1.346

2.9	37.4	24.4	30.9	13.0	55.759	3.900	1.255	1.283	0.706	1.242	0.744	1.280
4.0	42.3	24.9	33.6	17.4	57.362	5.009	1.213	1.228	0.676	1.212	0.713	1.249
5.1	46.7	24.9	35.8	21.8	57.946	6.071	1.167	1.197	0.658	1.194	0.694	1.230
5.9	50.7	25.1	37.9	25.6	56.940	6.920	1.110	1.186	0.652	1.188	0.688	1.224
6.9	54.4	25.2	39.8	29.2	58.694	7.672	1.115	1.183	0.651	1.187	0.686	1.222
7.8	57.7	25.3	41.5	32.4	59.313	8.321	1.104	1.186	0.653	1.189	0.688	1.224
9.1	61.8	25.3	43.6	36.5	60.959	9.095	1.110	1.195	0.658	1.194	0.693	1.229
Series II												
5.0	48.5	25.9	37.2	22.6	54.304	6.181	1.089	1.205	0.663	1.199	0.699	1.235
6.1	52.2	25.8	39.0	26.4	57.191	7.015	1.111	1.193	0.656	1.192	0.692	1.228
6.9	55.3	25.6	40.5	29.7	57.480	7.743	1.090	1.188	0.654	1.190	0.689	1.225
8.4	59.2	25.7	42.5	33.5	61.357	8.488	1.137	1.193	0.656	1.192	0.692	1.228
9.2	63.1	25.4	44.3	37.7	59.276	9.303	1.073	1.200	0.660	1.196	0.696	1.232
10.1	66.1	25.2	45.7	40.9	60.120	9.895	1.072	1.210	0.666	1.202	0.702	1.238
Average for the 15 results listed in this table							1.166	1.246	0.685	1.221	0.723	1.259
Average value for all 27 results shown in Figure 6							**1.197**	**1.239**	**0.682**	**1.218**	**0.719**	**1.255**

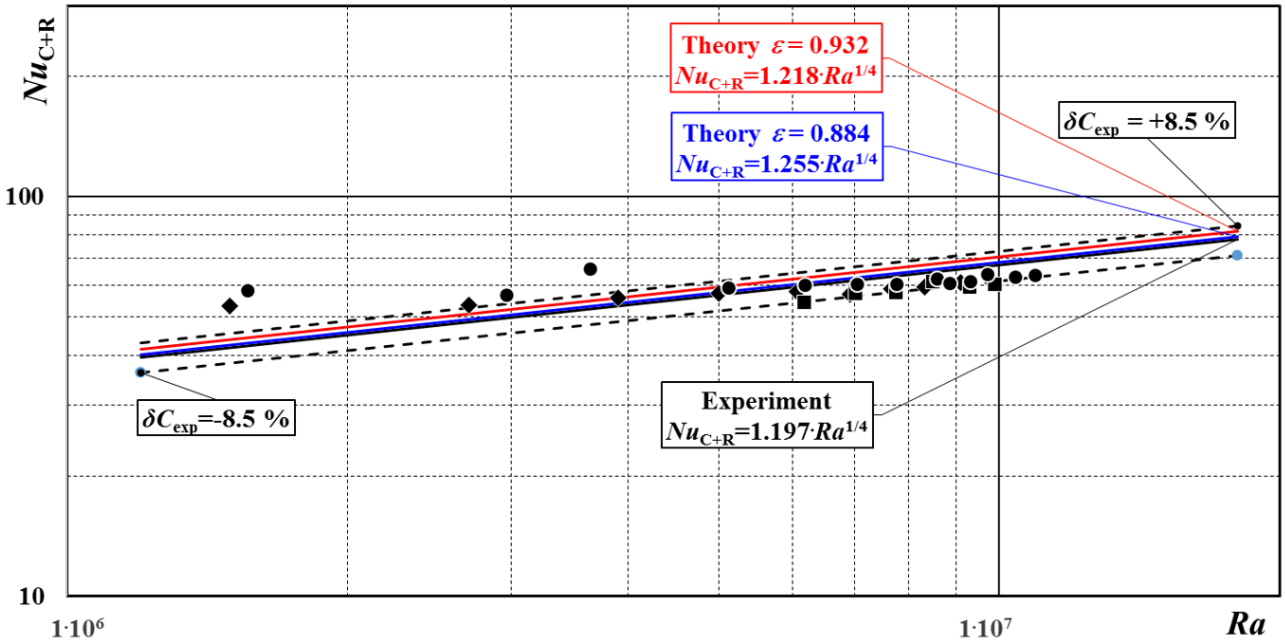

Figure 8. The results of the experimental tests, some of which - from Series I (diamonds) and Series II (squares) - are included in Table 3, and the remaining (Series III) experimental points (shown by dots) are not shown in Table 3. The black line shows the approximation of all the experimental results (41). The theoretical solution obtained for ε=0.884 is shown by the blue line, and the one for ε=0.932 by the red line

Further, from Eq. (37), the constant C_R was calculated for the two given for experimental plate emissivities ε=0.884 (estimated experimentally) and ε=0.932 (calculated from experimental data) [71] of a plate with a characteristic linear dimension of l=0.15 m. Without enquiring which of these emissivities is closer to reality, both values C_R and C_{C+R} were calculated.

The constant C_{C+R} is the sum of the convection constant C_C (40) and the radiation constant C_R:

$$C_{C+R} = C_C + C_R. \tag{41}$$

The results of these calculations were also subjected to double averaging with reference to the sample data listed in Table 3 and to all the results shown in Figure 8. The maximum relative uncertainty for the experiment in air ($\delta C_{exp.}$=±8.5%) has been adopted here.

At the end of the experimental research and theoretical considerations, it had to be checked whether the results fell within the laminar for air range $Ra < Ra_{cr,sir}=2\cdot10^8$ [79]. First, the experimental relationship (40) was checked: since this was obtained for water with the maximum number of $Ra_{max} \approx 8\cdot10^8 < Ra_{cr,water}=3.4\cdot10^9$ [79], it also raised no objections.

5. CONCLUSIONS

The results of the experimental studies published in the study [71] were used to validate the solution. Therefore, they cannot be suspected of being biased, even to a minimal degree. It is even more difficult to imagine the possibility of matching the results of theoretical considerations with experimental data. In this situation, the discrepancy between the experimental and theoretical values of $C_{C+R,av}$ – 1.75% (for ε=0.884) and 4.85% (for ε=0.932) – offers incontrovertible evidence confirming both the reliability of the experiment and the correctness of the solution of the empirical Eq. (39) with coefficient (36).

Having ensured that the solutions are correct, one can begin to outline its possible practical applications, which may be:

– a simple way of determining the heat loss from any external wall, building envelope, façade of a building, etc., or the heat flux transferred from internal walls inside a building, based on knowledge of: the value of its area A,

characteristic linear dimension l (height), temperature t_w, the surrounding temperature t_∞ and the approximate (e.g., tabular) value the surface emissivity ε, which has little effect on the result ($\Delta Q \approx 3\%$ for $\Delta\varepsilon$=0.05%).

– if the building surfaces under consideration are not vertical, isothermal or if $Ra > Ra_{cr}$ (C_C (20) or (40)), then it suffices to substitute the relevant values of C_C in Eq. (39).
– the development of dedicated software for a thermal imaging camera, which is based on the temperature of the heated surface t_w and the air in surrounding t_∞, which are in thermodynamic equilibrium with the surroundings, and the emissivities of the surface and the surroundings. With such a programme, a properly modified camera, in addition to its current applications in energy audits of buildings [62, 81-85], or recently for measuring air velocity [21], net heat flux [86] or heat flux and hot spot temperature in machining process [87], with the use of infrared image sequences, could also measure the total (convection-radiative) energy flux emitted from walls.

ACKNOWLEDGMENTS

This work was supported by the Icelandic Research Fund (Grant No. 184949); the Swedish Research Council (Grant No. 2020-05110).

REFERENCES

[1] Raznjevic, K. (1995). Handbook of Thermodynamic Tables. Begell House. New York.
[2] Handbook: Fundamentals - IP Edition. Atlanta: American Society of Heating, Refrigerating and Air-Conditioning Engineers. 2009. https://www.academia.edu/10884294/ASHRAE_handbook_fundamental, accessed on 15 March 2023.
[3] Modest, M.F. (2013). Radiative Heat Transfer. 3th Edition, McGraw-Hill, New York.
[4] Howell, J.R. Mengüc, M.P., Daun, K., Siegel R. (2021). Thermal Radiation Heat Transfer, 7th Edition, CRC Press.
[5] Ficker, T. (2019). General model of radiative and convective heat transfer in buildings: Part II: Convective and radiative heat losses. Acta Polytechnica, 59(3): 224-237. https://doi.org/10.14311/AP.2019.59.0224
[6] Karatas, H., Derbentli, T. (2018). Natural convection and radiation in rectangular cavities with one active vertical wall. International Journal of Thermal Sciences, 123: 129-139. https://doi.org/10.1016/j.ijthermalsci.2017.09.006
[7] Pudlik, W. (2012). Wymiana i Wymienniki Ciepła (Heat Transfer and Heat Exchangers) Gdańsk University of Tech. Publishing House, Gdańsk 2012, p. 232. https://pbc.gda.pl/Content/4404/wymiana-i-wymienniki-final.pdf.
[8] Stasiek, J. (1985). Application of the generalized configuration factors and the principle of surface transformation to radiant heat exchange in systems with optically active medium. Mechanika, 49: 386.
[9] Ozisik, M.N. (1987). Interaction of Radiation with Convection in Handbook of Single-phase Convective Heat Transfer. John Wiley & Sons, New York.
[10] Lewandowski, W.M., Khubeiz, J.M., Kubski, P., Bieszk, H., Wilczewski, T., Szymański, S. (1998). Natural convection heat transfer from complex surface. International Journal of Heat and Mass Transfer, 41(12): 1857-1868. https://doi.org/10.1016/s0017-9310(97)00240-8
[11] Misale, M., Fossa, M., Tanda, G. (2014). Investigation of free convection in a vertical water channel. Experimental Thermal and Fluid Science, 59: 252-257. https://doi.org/10.1016/j.expthermflusci.2014.01.022
[12] Lewandowski, W.M., Radziemska, E., Buzuk, M., Bieszk, H. (2000). Free convection heat transfer and fluid flow above horizontal rectangular plates. Applied Energy, 66(2): 177-197. https://doi.org/10.1016/S0306-2619(99)00024-0
[13] Lewandowski, W.M., Kubski, P., Bieszk, H. (1994). Heat transfer from polygonal horizontal isothermal surfaces. International Journal of Heat and Mass Transfer, 37(5): 855-864. https://doi.org/10.1016/0017-9310(94)90121-X
[14] Lewandowski, W.M., Bieszk, H., Cieslinski, J. (1992). Free convection from horizontal screened plates. Waerme-und Stoffuebertragung; (Germany), 27(8): 481-488. https://doi.org/10.1007/BF01590049
[15] Cieśliński, J., Pudlik, W. (1988). Laminar free-convection from spherical segments. International Journal of Heat and Fluid Flow, 9(4): 405-409. https://doi.org/10.1016/0142-727X(88)90007-0
[16] Lewandowski, W.M., Kubski, P., Khubeiz, J.M. (1993). Laminar free convection heat transfer from a horizontal ring. Wärme-und Stoffübertragung, 29(1): 9-16. https://doi.org/10.1007/BF01577454
[17] Cieśliński, J.T., Smolen, S., Sawicka, D. (2021). Free convection heat transfer from horizontal cylinders. Energies, 14(3): 559. https://doi.org/10.3390/en14030559
[18] Lewandowski, W.M., Kubski, P., Khubeiz, J.M. (1992). Natural convection heat transfer from round horizontal plate. Waerme-und Stoffuebertragung; (Germany), 27(5): 281-287. https://doi.org/10.1007/BF01589965
[19] Lewandowski, W.M., Ryms, M., Denda, H., Klugmann-Radziemska, E. (2014). Possibility of thermal imaging use in studies of natural convection heat transfer on the example of an isothermal vertical plate. International Journal of Heat and Mass Transfer, 78: 1232-1242. https://doi.org/10.1016/j.ijheatmasstransfer.2014.07.024
[20] Schaub, M., Kriegel, M., Brandt, S. (2019). Experimental investigation of heat transfer by unsteady natural convection at a vertical flat plate. International Journal of Heat and Mass Transfer, 136: 1186-1198. https://doi.org/10.1016/j.ijheatmasstransfer.2019.03.089
[21] Ryms, M., Tesch, K., Lewandowski, W.M. (2021). The use of thermal imaging camera to estimate velocity profiles based on temperature distribution in a free convection boundary layer. International Journal of Heat and Mass Transfer, 165: 120686. https://doi.org/10.1016/j.ijheatmasstransfer.2020.120686
[22] Lei, C., Patterson, J.C. (2003). A direct three-dimensional simulation of radiation-induced natural convection in a shallow wedge. International Journal of Heat and Mass Transfer, 46(7): 1183-1197. https://doi.org/10.1016/S0017-9310(02)00401-5
[23] Liu, X., Gong, G., Cheng, H. (2014). Combined natural convection and radiation heat transfer of various

absorbing-emitting-scattering media in a square cavity. Advances in Mechanical Engineering, 6: 403690. https://doi.org/10.1155/2014/403690
[24] Zhou, L., Liu, J., Huang, Q., Wang, Y. (2019). Analysis of combined natural convection and radiation heat transfer in a partitioned rectangular enclosure with semitransparent walls. Transactions of Tianjin University, 25: 472-487. https://doi.org/10.1007/s12209-019-00208-9
[25] Wang, Y., Yang, J., Zhang, X., Pan, Y. (2015). Effect of surface thermal radiation on natural convection and heat transfer in a cavity containing a horizontal porous layer. Procedia Engineering, 121: 1193-1199. https://doi.org/10.1016/j.proeng.2015.09.137
[26] Cabanillas, R.E., Estrada, C.A., Alvarez, G. (2002). Combined natural convection and radiation heat transfer in an open tilted cavity. WIT Transactions on Engineering Sciences, 35. https://doi.org/10.2495/HT020101
[27] Wang, Z., Yang, M., Li, L., Zhang, Y. (2011). Combined heat transfer by natural convection–conduction and surface radiation in an open cavity under constant heat flux heating. Numerical Heat Transfer, Part A: Applications, 60(4): 289-304. https://doi.org/10.1080/10407782.2011.594415
[28] Lugarini, A., Franco, A.T., Junqueira, S.L., Lage, J.L. (2018). Natural convection and surface radiation in a heated wall, C-shaped fracture. ASME Journal of Heat and Mass Transfer, 140(8): 082501. https://doi.org/10.1115/1.4039643
[29] Lacona, E., Taine, J. (2001). Holographic interferometry applied to coupled free convection and radiative transfer in a cavity containing a vertical plate between 290 and 650 K. International Journal of Heat and Mass Transfer, 44(19): 3755-3764. https://doi.org/10.1016/S0017-9310(01)00027-8
[30] Qasem, N.A.A., Imteyaz, B., Ben-Mansour, R., Habib, M.A. (2017). Effect of radiation heat transfer on naturally driven flow through parallel-plate vertical channel. Arabian Journal for Science and Engineering, 42: 1817-1829. https://doi.org/10.1007/s13369-016-2319-8
[31] Lewandowski, W.M., Ryms, M., Denda, H. (2017). Infrared techniques for natural convection investigations in channels between two vertical, parallel, isothermal and symmetrically heated plates. International Journal of Heat and Mass Transfer, 114: 958-969. https://doi.org/10.1016/j.ijheatmasstransfer.2017.06.120
[32] Lewandowski, W.M., Ryms, M., Denda, H. (2018). Natural convection in symmetrically heated vertical channels. International Journal of Thermal Sciences, 134: 530-540. https://doi.org/10.1016/j.ijthermalsci.2018.08.036
[33] Krishna Sabareesh, R., Prasanna, S., Venkateshan, S.P. (2010). Investigations on multimode heat transfer from a heated vertical plate. Journal of Heat Transfer, 132(3): 032501. https://doi.org/10.1115/1.4000055
[34] Shati, A.K.A., Blakey, S.G., Beck, S.B.M. (2012). A dimensionless solution to radiation and turbulent natural convection in square and rectangular enclosures. Journal of Engineering Science and Technology, 7(2): 257-279.
[35] Pantokratoras, A. (2014). Natural convection along a vertical isothermal plate with linear and non-linear Rosseland thermal radiation. International Journal of Thermal Sciences, 84: 151-157. https://doi.org/10.1016/j.ijthermalsci.2014.05.015
[36] Cheesewright, R. (1968). Turbulent natural convection from a vertical plane surface. ASME Journal of Heat and Mass Transfer, 90(1): 1-6. https://doi.org/10.1115/1.3597453
[37] Hasan, M.M., Eichhorn, R. (1979). Local nonsimilarity solution of free convection flow and heat transfer from an inclined isothermal plate. ASME Journal of Heat and Mass Transfer, 101(4): 642-647. https://doi.org/10.1115/1.3451050
[38] Fujii, T., Imura, H. (1972). Natural-convection heat transfer from a plate with arbitrary inclination. International Journal of Heat and Mass Transfer, 15(4): 755-767. https://doi.org/10.1016/0017-9310(72)90118-4
[39] Hossain, M.A., Takhar, H.S. (1996). Radiation effect on mixed convection along a vertical plate with uniform surface temperature. Heat and Mass Transfer, 31(4): 243-248. https://doi.org/10.1007/BF02328616
[40] Cao, K., Baker, J. (2015). Non-continuum effects on natural convection–radiation boundary layer flow from a heated vertical plate. International Journal of Heat and Mass Transfer, 90: 26-33. https://doi.org/10.1016/j.ijheatmasstransfer.2015.05.014
[41] Arpaci, V.S. (1968). Effect of thermal radiation on the laminar free convection from a heated vertical plate. International Journal of Heat and Mass Transfer, 11(5): 871-881. https://doi.org/10.1016/0017-9310(68)90130-0
[42] Reddy, M.G. (2014). Influence of thermal radiation, viscous dissipation and hall current on MHD convection flow over a stretched vertical flat plate. Ain Shams Engineering Journal, 5(1): 169-175. https://doi.org/10.1016/j.asej.2013.08.003
[43] Venugopal, G., Deiveegan, M., Balaji, C., Venkateshan, S.P. (2008). Simultaneous retrieval of total hemispherical emissivity and specific heat from transient multimode heat transfer experiments. Journal of Heat Transfer, 130(6): 061601. https://doi.org/10.1115/1.2891221
[44] Venugopal, G., Balaji, C., Venkateshan, S.P. (2008). A correlation for laminar mixed convection from vertical plates using transient experiments. Heat and Mass Transfer, 44(12): 1417-1425. https://doi.org/10.1007/s00231-008-0380-x
[45] Bhowmik, H., Faisal, A. (2017). Experimental analyses of natural convection and radiation heat transfer from a horizontal cylinder. 10th International Conference on Thermal Engineering: Theory and Applications, February 26-28, 2017, Muscat, Oman, pp. 1-5.
[46] Popiel, C.O., Wojtkowiak, J., Bober, K. (2007). Laminar free convective heat transfer from isothermal vertical slender cylinder. Experimental Thermal and Fluid Science, 32(2): 607-613. https://doi.org/10.1016/j.expthermflusci.2007.07.003
[47] Kobus, C.J., Wedekind, G.L. (1995). An experimental investigation into forced, natural and combined forced and natural convective heat transfer from stationary isothermal circular disks. International Journal of Heat and Mass Transfer, 38(18): 3329-3339. https://doi.org/10.1016/0017-9310(95)00096-R
[48] Ali, M. (2009). Natural convection heat transfer along vertical rectangular ducts. Heat and Mass Transfer, 46: 255-266. https://doi.org/10.1007/s00231-009-0561-2
[49] Zeyghami, M., Rahman, M.M. (2015). Analysis of

combined natural convection and radiation heat transfer using a similarity solution. Energy Research Journal, 6(2): 64-73. https://doi.org/10.3844/erjsp.2015.64.73
[50] Jannot, M., Kunc, T. (1998). Onset of transition to turbulence in natural convection with gas along a vertical isotherm plane. International Journal of Heat and Mass Transfer, 41(24): 4327-4340. https://doi.org/10.1016/S0017-9310(98)00068-4
[51] Clausing, A.M., Berton, J.J. (1989). An experimental investigation of natural convection from an isothermal horizontal plate. ASME Journal of Heat and Mass Transfer, 111(4): 904-908. https://doi.org/10.1115/1.3250804
[52] Eckert, E.R.G., Jackson, T.W. (1950). Analysis of turbulent free-convection boundary layer on flat plate (No. NACA-TN-2207).
[53] Hossain, M.A., Rees, D.A.S., Pop, I. (1998). Free convection-radiation interaction from an isothermal plate inclined at a small angle to the horizontal. Acta Mechanica, 127(1-4): 63-73. https://doi.org/10.1007/BF01170363
[54] Cess, R.D. (1966). The interaction of thermal radiation with free convection heat transfer. International Journal of Heat and Mass Transfer, 9(11): 1269-1277. https://doi.org/10.1016/0017-9310(66)90119-0
[55] England, W.G., Emery, A.F. (1969). Thermal radiation effects on the laminar free convection boundary layer of an absorbing gas. ASME Journal of Heat and Mass Transfer, 91(1): 37-44. https://doi.org/10.1115/1.3580116
[56] Ramesh, N., Balaji, C., Venkateshan, S.P. (2000). Effect of radiation on natural convection in an L-shaped corner. Experiments in Fluids, 28(5): 448-454. https://doi.org/10.1007/s003480050404
[57] Kimura, K. (2016). Scientific Basis of Air Conditioning. Edition: Second Edition 2016 Publisher: International Research Institute on Human Environment ISBN: 978-4-9907042-3-0.
[58] Lewandowski, W.M., Lewandowska-Iwaniak, W. (2014). The external walls of a passive building: A classification and description of their thermal and optical properties. Energy and Buildings, 69: 93-102. https://doi.org/10.1016/j.enbuild.2013.10.021
[59] Sobota, T., Taler, J. (2018). Determination of heat losses through building partitions. In MATEC Web of Conferences, 240: 05030. https://doi.org/10.1051/matecconf/201824005030
[60] Ficker, T. (2019). General model of radiative and convective heat transfer in buildings: Part I: Algebraic model of radiative heat transfer. Acta Polytechnica, 59(3): 211-223. https://doi.org/10.14311/AP.2019.59.0211
[61] Kulacki, F.A., Nagle, M.E., Cassen, P. (1974). Studies of heat source driven natural convection (No. NASA-TM-X-70232). Technical Report 3746-2, Grant NGR 36-008-205.
[62] Ohlsson, K.E.A., Olofsson, T. (2014). Quantitative infrared thermography imaging of the density of heat flow rate through a building element surface. Applied Energy, 134: 499-505. https://doi.org/10.1016/j.apenergy.2014.08.058
[63] Wernik, J. (2017). Investigation of heat loss from the finned housing of the electric motor of a vacuum pump. Applied Sciences, 7(12): 1214. https://doi.org/10.3390/app7121214
[64] Sakin, M., Kaymak-Ertekin, F., Ilicali, C. (2009). Convection and radiation combined surface heat transfer coefficient in baking ovens. Journal of Food Engineering, 94(3-4): 344-349. https://doi.org/10.1016/j.jfoodeng.2009.03.027
[65] Parra, C.A.F. (2008). Heat transfer investigations in a modern diesel engine. Doctoral dissertation, University of Bath.
[66] Rantala, M. (2015). Heat transfer phenomena in float glass heat treatment processes. Tampere University of Technology, Publication, Vuosikerta, pp. 1-135.
[67] Rantala M. (2019). Thermal Radiation and Forced Convection in Flat Glass Tempering Furnaces, Glaston Finland Oy, GPD Tempere, Finland (The Glass Performance Days). https://www.glassonweb.com/article/thermal-radiation-and-forced-convection-flat-glass-tempering-furnaces.
[68] Lewandowski, W.M., Ryms, M., Denda, H. (2018). Quantitative study of free convective heat losses from thermodynamic partitions using Thermal Imaging. Energy and Buildings, 167: 370-383. https://doi.org/10.1016/j.enbuild.2017.12.047
[69] Minkina, W., Dudzik, S. (2009). Infrared Thermography: Errors and Uncertainties. John Wiley & Sons. https://doi.org/10.1002/9780470682234
[70] Dudzik, S., Minkina, W. (2018). Examples of uncertainty calculations in thermographic measurements. Przegląd Elektrotechniczny, 94: 124-129. https://doi.org/10.15199/48.2018.12.26
[71] Ryms M., Lewandowski, W.M. (2021). Evaluating the influence of radiative heat flux on convective heat transfer from a vertical plate in air using an improved heating plate. International Journal of Heat and Mass Transfer, 173: 121232. https://doi.org/10.1016/j.ijheatmasstransfer.2021.121232
[72] Pohlhausen, E. (1921). Der Wärmeaustausch zwischen festen Körpern und Flüssigkeiten mit kleiner Reibung und kleiner Wärmeleitung. ZAMM-Journal of Applied Mathematics and Mechanics/Zeitschrift für Angewandte Mathematik und Mechanik, 1(2): 115-121. https://doi.org/10.1002/zamm.19210010205
[73] Saunders, O.A. (1936). The effect of pressure upon natural convection in air. Proceedings of the Royal Society of London. Series A-Mathematical and Physical Sciences, 157(891): 278-291. https://doi.org/10.1098/rspa.1936.0194
[74] Mikheyev, M.A. (1956). Principals of Heat Transfer of heat transfer. Principals of Heat Transfer, 3rd Edition, Gosenergoizdat Publ. House.
[75] Lewandowski, W.M., Kubski, P. (1983). Methodical investigation of free convection from vertical and horizontal plates. Heat and Mass Transfer, 17(3): 147-154.
[76] Domański R., Jaworski M., Rebrow M. (2000). Heat Transfer - Computer aided calculations: tables of thermophysical properties, Wydawnictwo Politechniki Warszawskiej 2000 /in Polish https://repo.pw.edu.pl/info/book/WUT287656/.
[77] Thermal Fluid Properties Calculator http://www.mhtl.uwaterloo.ca/RScalculators.html/, accessed on 15 March 2023.
[78] Ryms, M., Kwiatkowski, G.J., Lewandowski, W.M. (2022). On the differential effect of temperature on the

Nusselt-Rayleigh relationship in free convection. International Journal of Thermal Sciences, 181: 107744. https://doi.org/10.1016/j.ijheatmasstransfer.2021.122264
[79] Bejan, A., Lage, J.L. (1990). The Prandtl number effect on the transition in natural convection along a vertical surface. Journal of Heat Transfer, 112(3): 787-790.
[80] Corcione, M., Habib, E., Campo, A. (2011). Natural convection from inclined plates to gases and liquids when both sides are uniformly heated at the same temperature. International Journal of Thermal Sciences, 50(8): 1405-1416. https://doi.org/10.1016/j.ijthermalsci.2011.03.012
[81] Fokaides, P.A., Kalogirou, S.A. (2011). Application of infrared thermography for the determination of the overall heat transfer coefficient (U-Value) in building envelopes. Applied Energy, 88(12): 4358-4365. https://doi.org/10.1016/j.apenergy.2011.05.014
[82] Plesu, R., Teodoriu, G., Taranu, G. (2012). Infrared thermography applications for building investigation. Buletinul Institutului Politehnic Din Lasi. Sectia Constructii, Arhitectura, 58(1): 157-168.
[83] Albatici, R., Tonelli, A.M., Chiogna, M. (2015). A comprehensive experimental approach for the validation of quantitative infrared thermography in the evaluation of building thermal transmittance. Applied Energy, 141: 218-228. https://doi.org/10.1016/j.apenergy.2014.12.035
[84] Kylili, A., Fokaides, P.A., Christou, P., Kalogirou, S.A. (2014). Infrared thermography (IRT) applications for building diagnostics: A review. Applied Energy, 134: 531-549. https://doi.org/10.1016/j.apenergy.2014.08.005
[85] Hoyano, A., Asano, K., Kanamaru, T. (1999). Analysis of the sensible heat flux from the exterior surface of buildings using time sequential thermography. Atmospheric Environment, 33(24-25): 3941-3951. https://doi.org/10.1016/S1352-2310(99)00136-3
[86] Garbe, C.S., Spies, H., Jähne, B. (2003). Estimation of surface flow and net heat flux from infrared image sequences. Journal of Mathematical Imaging and Vision, 19(3): 159-174. https://doi.org/10.1023/A:1026233919766
[87] da Silva, R.G.D., Ferreira, D.C., Dutra, F.V.A., e Silva, S.M.M.L. (2021). Simultaneous real time estimation of heat flux and hot spot temperature in machining process using infrared camera. Case Studies in Thermal Engineering, 28: 101352. https://doi.org/10.1016/j.csite.2021.101352

NOMENCLATURE

a	coefficient of thermal diffusivity, m^2/s
A	surface area, m^2
b	width of the plate, m
$B1$	function, $K \cdot m^{7/4}/W$ (29), (32)
$B2$	function, $W/(m^2 \cdot K)$ (30), (33)
c_p	specific heat, $J/(kg \cdot K)$
C	coefficient in the Rayleigh–Nusselt equation
g	acceleration due to gravity, m/s^2
h	height of the plate, m
I	current, A
l	characteristic length, m
n	exponent
N	heater power, W
Nu	Nusselt number, dimensionless
Ra	Rayleigh number, dimensionless
t,T	temperature, °C, K
q	flux density, W/m^2
Q	heat flux, W
U	voltage, V

Greek symbols

α	heat-transfer coefficient, $W/(m^2 \cdot K)$
β	coefficient of thermal expansion, 1/K
δ	uncertainty
ε	surface emissivity
σ	Stefan-Boltzmann constant, $W/(m^2 \cdot K^4)$
Δ	difference
λ	thermal conductivity, $W/(m \cdot K)$
μ	dynamic viscosity, $kg/(m \cdot s)$
ρ	density, kg/m^3
ν	kinematic viscosity, m^2/s

Subscripts

av	average
cr	critical
C	convective
in	inlet
max	maximum
loss	losses
out	outlet
R	radiative
w	wall
∞	in surroundings